Article

Impacts of Ni-Loading Method on the Structure and the Catalytic Activity of NiO/SiO$_2$-Al$_2$O$_3$ for Ethylene Oligomerization

Katsuya Shimura [1],*, Shigehiro Yoshida [2], Hiroshi Oikawa [2] and Tadahiro Fujitani [1]

[1] Interdisciplinary Research Center for Catalytic Chemistry, National Institute of Advanced Industrial Science and Technology (AIST), 1-1-1 Higashi, Tsukuba 305-8565, Ibaraki, Japan; t-fujitani@aist.go.jp
[2] Innovative Research Excellence, Power Unit & Energy, Honda R & D Co., Ltd., 3-15-1 Senzui, Asaka 351-0024, Saitama, Japan; shigehiro_yoshida@jp.honda (S.Y.); hiroshi_oikawa@jp.honda (H.O.)
* Correspondence: katsuya-shimura@aist.go.jp; Tel.: +81-82-493-6844

Abstract: To clarify the Ni species of NiO/SiO$_2$-Al$_2$O$_3$ catalysts that are active for ethylene oligomerization, 18 types of NiO/SiO$_2$-Al$_2$O$_3$ were prepared using three Ni-loading methods (i.e., ion-exchange, impregnation, and homogeneous precipitation), with different Ni-loadings (1–20 wt%), and examined with respect to their structure and catalytic activity for ethylene oligomerization. Characterized by N$_2$ adsorption, powder XRD, FE-SEM, H$_2$-TPR, NH$_3$-TPD, and C$_2$H$_4$-TPD showed that Ni species in the catalysts prepared by ion-exchange were mainly ion-exchanged Ni cations. In contrast, Ni species in the catalysts prepared by impregnation were a mixture of ion-exchanged Ni cations and NiO particles, and those in the catalysts prepared by homogeneous precipitation were all NiSiO$_3$ particles. Catalytic-reaction tests at 300 °C and 0.1 MPa revealed the following: the ion-exchanged Ni cations showed the highest C$_2$H$_4$ conversion rate; the NiSiO$_3$ particles showed a moderate reaction rate; and the NiO particles were not active for ethylene oligomerization. We concluded that the high catalytic activity of the ion-exchanged Ni cations was a result of their high dispersion and medium-strength acidity, which together promoted the adsorption and activation of ethylene on, and the desorption of oligomerization products from, the catalyst.

Keywords: ethylene oligomerization; NiO/SiO$_2$-Al$_2$O$_3$ catalyst; ion-exchange; impregnation; homogeneous precipitation

1. Introduction

With the gradual maturation of technologies for producing ethylene using resources other than petroleum (e.g., dehydrogenation of ethane derived from shale gas, bioethanol conversion to ethylene by catalytic dehydration, and the zeolite-catalyzed methanol-to-olefin (MTO) process), the production of chemicals and liquid fuels from ethylene has attracted renewed attention [1–3]. Oligomerization of ethylene into long-chain olefins is one of the important reactions required for ethylene conversion and has been applied in the production of chemical intermediates, base materials, and liquid fuels [1,4–6]. Currently, several million tons of linear α-olefins are produced by homogeneously-catalyzed ethylene oligomerization (EO), which comprises transition metal complexes, alkylaluminum cocatalysts, and organic solvents. Among others, the following processes have been commercialized for the manufacturing of linear α-olefins [7,8]: the Shell higher olefin process (SHOP), which uses a nickel complex; the Alphabutol process, which uses a titanium complex; and the SABIC/Linde Alpha-SABLIN process, which uses a zirconium complex. However, these homogeneous catalysts suffer from several drawbacks, including a high difficulty in the separation of the product from the solvent, a high sensitivity to impurities, and limited catalyst reusability. Thus, a heterogenous catalytic process that does not require any cocatalysts or solvents and is easy to handle and recycle is needed.

Ni-containing catalysts, microporous and mesoporous catalysts, and solid acid catalysts have been extensively studied as heterogeneous catalysts for EO; examples of such catalysts include the following: nickel ion-exchanged zeolites (e.g., Y [6,9,10], beta [11–14], ZSM-5 [15,16], MCM-22 [17,18], MCM-36 [17,18]); nickel-loaded amorphous silica–alumina (ASA) [5,19–27]; Ni-exchanged cationic clay [28]; Ni-containing ordered mesoporous silica–alumina (e.g., Al-MCM-41 [29–32], Al-SBA-15 [33–36], Al-KIT-6 [37,38]); nickel sulfate ($NiSO_4$) supported on Al_2O_3 [39–42], ASA [43], ZrO_2 [44] or TiO_2 [44]; and nickel phosphide (Ni_2P) supported on ASA [45] or SiO_2 [46]. These catalysts are easy to handle and recycle, and they do not need any promoters or solvents (except for Ni_2P catalysts). It is well known that, in heterogeneous catalytic systems, the pore size of the support greatly influences the catalytic activity and lifetime. For example, Ni-zeolite catalysts, except for Ni-beta, often deactivate rapidly due to the blocking of the zeolites' micropores by bulky and highly-branched oligomers that formed during the reaction [11,16–18]. In contrast, Ni-containing mesoporous silica–alumina catalysts, such as Ni-exchanged ASA [22,23], Ni-Al-MCM-41 [29,30], and Ni-Al-SBA-15 [33,34], show a high and stable activity. In recent years, heterogeneous catalysts with a performance competitive to that of homogeneous catalysts have been reported by several research groups [1,30,34]; however, most heterogeneous catalytic systems cannot produce linear α-olefins selectively because consecutive reactions of the produced oligomers (e.g., cracking, isomerization, and aromatization) occur over the strong acidic sites of aluminosilicate support. In addition, gradual deactivation often occurs over heterogeneous catalysts owing to the coke deposition. Thus, improved catalysts are needed for the development of commercialized heterogeneous catalytic systems.

To improve the catalytic performance of heterogeneous Ni catalysts for EO, we need to precisely control both the size and oxidation state of the NiO particles. Previously, it was proposed that isolated Ni^{2+} cations in ion-exchanged positions were the active Ni species for EO and that large NiO particles were inactive [11,20,30,47]. However, the detailed studies based on Fourier-transform infrared spectroscopy (FT-IR) coupled with low-temperature CO adsorption have suggested that isolated Ni^{2+} cations grafted on acidic silanols and under-coordinated Ni^{2+} cations on sub-5 nm NiO nanoparticles were active sites for Ni-beta [12], Ni-Al-MCM-41 [31], and Ni-loaded ASA [27,48]. Density functional theory (DFT)-based molecular dynamics simulations have suggested a mobile $[(ethylene)_2-Ni-(alkyl)]^+$ species in the zeolite micropores as the active Ni species in EO over the Ni-SSZ-24 catalyst [49]. It has also been suggested that, in Ni ion-exchanged zeolite beta catalysts, bent mono(μ-oxo) dinickel ($[Ni-O-Ni]^{2+}$) complexes showed higher activity than ion-exchanged Ni ions [13]. The oxidation state of Ni has also been studied by various groups, and monovalent Ni^+ was previously thought to be an active Ni species [34,39,41–44,50]; however, recent computational and experimental investigations revealed that Ni^{2+} cations were the plausible active sites for the oligomerization of light olefins [11–14,31,47,48,51,52]. Thus, various studies have been conducted to clarify the active Ni species, but consensus is yet to be reached regarding the types of active Ni species.

Previously, we studied the impacts of the preparation method used to synthesize the ASA support on the catalytic performance of NiO/ASA (Ni/ASA) for EO [53,54]. The ASA supports were prepared from tetraethyl orthosilicate and aluminum nitrate nonahydrate using the coprecipitation or the homogeneous precipitation method. Forty-nine types of ASA with different pore sizes and acidic site amounts were synthesized by varying the preparation conditions. NiO particles were deposited on the supports by the impregnation of the $Ni(NO_3)_2 \cdot 6H_2O$ precursor, followed by calcination. When we systematically studied the relationships between the structure and the activity of the Ni/ASA catalysts, we found that C_2H_4 conversion of the Ni/ASA catalysts increased when increasing the acidic sites amounts. This result suggests that proximity of the Ni cations to the surface acidic sites of the ASA support greatly improves the catalytic activity. In addition, C_2H_4 conversion increased when decreasing the density of surface Ni sites, indicating that highly dispersed Ni species (e.g., Ni cations in ion-exchanged position and small NiO nanoparticles) may have superior catalytic activity compared to large NiO particles.

In this study, the Ni/ASA catalysts were prepared using three different Ni-loading methods: impregnation, ion-exchange, and one-step homogeneous precipitation. Impregnation and ion-exchange have been frequently used as the preparation methods of heterogeneous Ni catalysts and were thus employed in this study. One-step homogeneous precipitation was also examined, since we expected that it would be effective for the formation of highly dispersed Ni species. By changing the preparation method and Ni-loading, we obtained 18 types of Ni/ASA catalysts with different Ni species and then examined the relationship between the types of Ni species and the C_2H_4 conversion rate. In these catalysts, we found the following: the ion-exchanged Ni species showed the highest C_2H_4 conversion rate; the $NiSiO_3$ particles showed a moderate reaction rate; and the NiO particles were not active for EO.

2. Results and Discussion

2.1. Catalytic Activity of Ni/ASA Prepared Using Different Ni-Loading Methods

The catalytic activity of Ni/ASA for EO was evaluated at 300 °C, 0.1 MPa, and a gas hourly space velocity (GHSV) of 12 L/$g_{cat.}$/h. Table 1 shows the results of catalytic reactions obtained with the ASA support alone, Ni/ASA catalysts with different Ni-loadings and preparation methods, and $NiSiO_3$ alone. For all the Ni/ASA catalysts, the main products of EO were C_4 (1-C_4H_8, 2-C_4H_8, and iso-C_4H_8), C_6 (12 types of C_6H_{12}), C_5 (5 types of C_5H_{10}), and C_3H_6 hydrocarbons (Table 1). C_4 and C_6 olefins were produced by dimerization and trimerization of ethylene on the Ni sites, respectively, whereas C_3 and C_5 olefins were mainly produced by secondary cracking reactions of long-chain oligomers (e.g., C_8H_{16} → C_3H_6 + C_5H_{10}, C_6H_{12} → $2C_3H_6$) on the acidic sites of the ASA support [53,54]. The remaining products were C_{7+} hydrocarbons; however, the sum of the selectivity for the C_{7+} hydrocarbons was below 10% in most catalysts. This is because reactions at low pressure and low C_2H_4 conversion suppressed the formation of long-chain hydrocarbons with seven or more carbon atoms. Over the bare ASA support, EO proceeded at a very low rate, and C_2H_4 conversion and C_4 yield were 0.58% and 0.10%, respectively (Table 1, Entry 1). The low catalytic activity of the ASA was due to the instability of the primary $C_2H_5^+$ carbonium cation intermediates that formed on the Brønsted acid sites of the aluminosilicate carrier during EO [11,31].

Ni-loading greatly increased the reaction rate for EO. Over the Ni/ASA catalysts prepared using impregnation (Ni Imp), C_2H_4 conversion and C_4 yield first increased with an increase in Ni-loading up to 0.5 wt%, and then remained constant up to 8 wt% (Table 1, Entries 2–9, and Figure 1a). This result indicates that Ni species formed under low Ni-loading conditions (≤0.5 wt%) are the main contributors to EO, whereas those formed under high Ni-loading conditions (>1 wt%) are not. Among the Ni Imp catalysts, the highest C_2H_4 conversion (27.1%) was obtained over Ni(0.5) Imp (Entry 4), and the highest C_4 yield (21.3%) was obtained over Ni(6) Imp (Entry 8).

A different dependency between Ni-loading and catalytic activity was observed over Ni/ASA catalysts prepared using one-step homogeneous precipitation (Ni HP). The C_2H_4 conversion and C_4 yield first increased with an increase in Ni-loading up to 6 wt%, then became constant at 6–12 wt%, and finally decreased at >12 wt% (Table 1, Entries 10–18 and Figure 1b). This difference in the optimum Ni-loading compared to that of the Ni Imp catalyst indicates that the nature of the Ni species in the two types of catalyst differs. Among the Ni HP catalysts, Ni(6) HP showed the highest activity (Entry 13): the C_2H_4 conversion and C_4 yield over Ni(6) HP were 24.5% and 19.5%, respectively, which were lower than those of the best Ni Imp catalyst.

Table 1. Catalytic activity of ASA support, Ni/ASA catalysts, and NiSiO$_3$ for EO [a].

Entry	Catalyst	Conv. C_2H_4 (%)	Yield [b] (%)				Selectivity [b] (%)				Iso-C_4H_8/n-C_4H_8 [c]
			C3	C4	C5	C6	C3	C4	C5	C6	
1	ASA	0.58	0.00	0.10	0.00	0.03	0.0	18.0	0.0	5.7	0.67
2	Ni(0.1) Imp	9.73	0.00	8.21	0.22	0.70	0.0	84.4	2.3	7.2	0.30
3	Ni(0.3) Imp	18.14	0.37	15.06	0.42	1.48	2.1	83.0	2.3	8.2	0.28
4	Ni(0.5) Imp	27.12	0.66	21.06	0.52	2.01	2.4	77.6	1.9	7.4	0.21
5	Ni(1) Imp	26.30	0.64	20.95	0.51	1.99	2.4	79.7	1.9	7.6	0.21
6	Ni(2) Imp	26.43	0.66	20.64	0.53	2.04	2.5	78.1	2.0	7.7	0.21
7	Ni(4) Imp	24.66	0.63	19.79	0.48	1.88	2.5	80.3	1.9	7.6	0.21
8	Ni(6) Imp	26.79	0.56	21.27	0.45	1.97	2.1	79.4	1.7	7.4	0.21
9	Ni(8) Imp	22.70	0.49	19.20	0.42	1.78	2.2	84.6	1.8	7.8	0.21
10	Ni(1) HP	14.74	0.22	11.23	0.31	1.08	1.5	76.2	2.1	7.3	0.28
11	Ni(2) HP	13.79	0.24	11.09	0.32	1.01	1.8	80.4	2.3	7.3	0.29
12	Ni(4) HP	18.53	0.46	15.14	0.47	1.54	2.5	81.7	2.5	8.3	0.27
13	Ni(6) HP	24.49	0.52	19.46	0.49	1.85	2.1	79.5	2.0	7.5	0.21
14	Ni(8) HP	24.52	0.64	19.42	0.55	1.91	2.6	79.2	2.2	7.8	0.21
15	Ni(10) HP	24.38	0.57	18.96	0.47	1.79	2.4	77.8	1.9	7.3	0.21
16	Ni(12) HP	23.30	0.60	19.28	0.47	1.86	2.6	82.8	2.0	8.0	0.21
17	Ni(16) HP	18.10	0.44	14.69	0.35	1.47	2.4	81.2	1.9	8.1	0.26
18	Ni(20) HP	16.17	0.39	13.35	0.32	1.35	2.4	82.5	2.0	8.4	0.26
19	Ni(1.1) IE	31.14	0.80	24.76	0.57	2.39	2.6	79.5	1.8	7.7	0.21
20	NiSiO$_3$	2.01	0.00	1.87	0.00	0.06	0.0	93.0	0.1	3.0	0.31

[a] Conditions: Catalyst: 0.2 g, temperature: 300 °C, pressure: 0.1 MPa, C$_2$H$_4$: 20 mL/min, N$_2$: 20 mL/min. [b] C3: propylene, C4: butene, C5: pentene, C6: hexene. [c] Ratio of isobutene to normal butene.
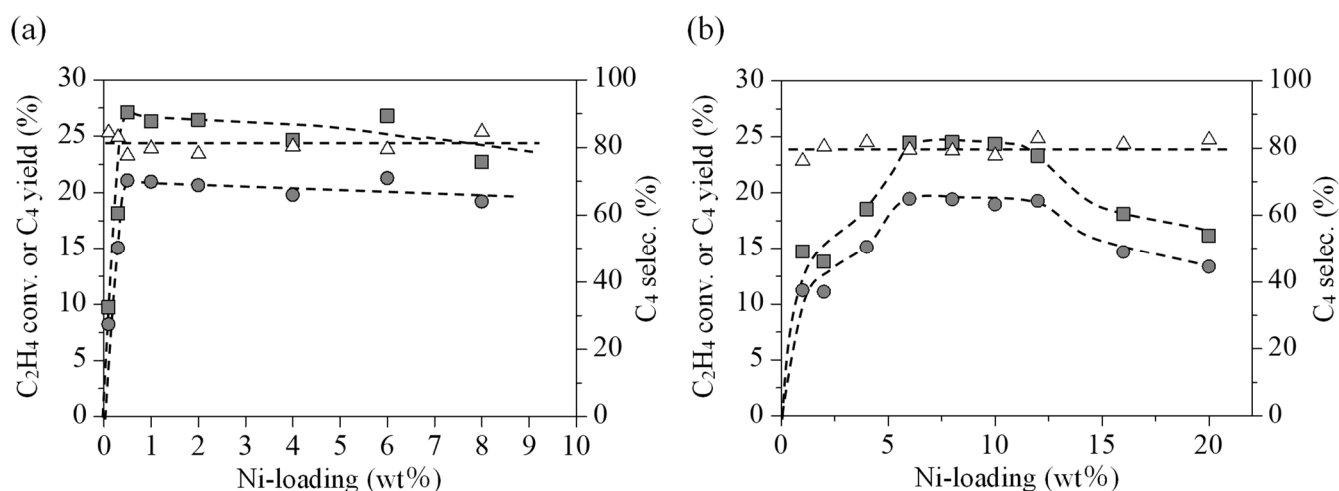

Figure 1. C$_2$H$_4$ conversion (gray squares), C$_4$ yield (gray circles), and C$_4$ selectivity (white triangles) over Ni/ASA catalysts prepared by an (**a**) impregnation or (**b**) one-step homogeneous precipitation method of Ni-loading. Conditions: Catalyst: 0.2 g, temperature: 300 °C, pressure: 0.1 MPa, C$_2$H$_4$: 20 mL/min, N$_2$: 20 mL/min.

Comparing the Ni/ASA catalysts prepared using ion-exchange (Ni IE), Ni(0.5) Imp, and Ni(6) HP, Ni IE showed higher activity than both the other catalysts (Table 1, Entry 19, and Figure 2). The C$_2$H$_4$ conversion and C$_4$ yield over Ni IE were 31.1% and 24.8%, respectively. These values were much higher than those of Ni-Al-SBA-15 (C$_2$H$_4$ conversion: 20.6%; and C$_4$ yield: 16.7%) [53], which was one of the best heterogeneous catalysts for EO reported to date [33,34]. The activity of Ni IE was also compared with that of the previously reported heterogeneous catalysts (Table S1). It was found that Ni IE exhibited the best performance at 0.1 MPa.
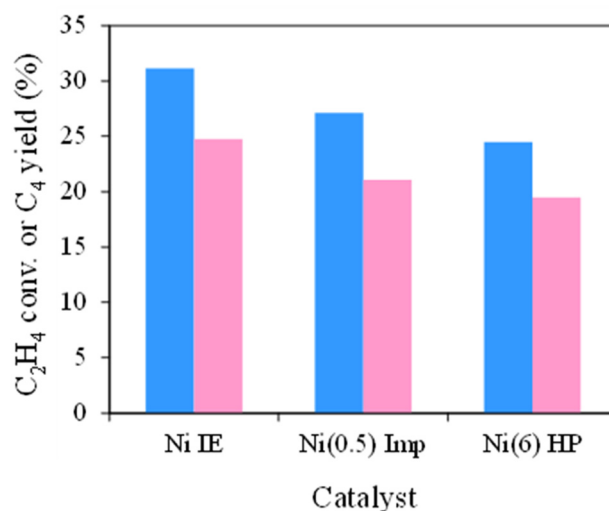
Figure 2. Comparison of C_2H_4 conversion (blue bar) and C_4 yield (pink bar) over Ni/ASA catalysts prepared using an ion-exchange (IE), impregnation (Imp), or one-step homogeneous precipitation (HP) method of Ni-loading. Conditions: Catalyst: 0.2 g, temperature: 300 °C, pressure: 0.1 MPa, C_2H_4: 20 mL/min, N_2: 20 mL/min.

For all the catalysts, the C_4 selectivity was around 80% and was not influenced by the Ni-loading or preparation method (Table 1 and Figure 1). Constant C_4 selectivity at a low C_2H_4 conversion (<30%) has been reported by several other research groups (e.g., EO over Ni-exchanged ASA [24] and $NiSO_4$-loaded Al_2O_3 [47]). The ratio of isobutene to normal butene over the Ni/ASA catalysts was also constant, in the range of 0.21–0.30 (Table 1).

The time-course of C_2H_4 conversion over the Ni IE catalyst was compared to that over two representative Ni Imp and Ni HP catalysts (Figure S1). For each of the three catalysts, C_2H_4 conversion gradually decreased with time on stream, which we attributed to coke deposition. However, the rate of activity decrease was slower over the Ni IE catalyst than over the Ni Imp and Ni HP catalysts, indicating that the Ni IE catalyst not only had a higher catalytic activity, but also a higher resistance to catalyst deactivation compared to the other catalysts. We also carried out the catalyst-recycling test. The C_2H_4 conversion and C_4 yield of the Ni IE catalyst were fully recovered by calcining the used catalyst in air at 500 °C for 3 h. This result may indicate that the structure and oxidation state of Ni species do not change during the reaction for at least 5 h.

The effects of reaction-temperature on catalytic activity were examined in five of the Ni/ASA catalysts covering the ranges of Ni-loadings and preparation methods used: Ni(1.1) IE, Ni(1) Imp, Ni(8) Imp, Ni(8) HP, and Ni(12) HP. The equilibrium conversion of ethylene dimerization under the present reaction conditions (200–300 °C and 0.1 MPa) exceeded 98%. For all the catalysts, the C_2H_4 conversion and C_4 yield monotonically increased with an increase in the reaction temperature from 200 to 300 °C, as shown for the Ni IE catalyst in Figure 3. However, the C_4 selectivity decreased with the increasing reaction temperature, probably because consecutive reactions of the C_4H_8 on the acidic sites of the ASA support (e.g., oligomerization, alkylation, and cracking) were promoted at higher temperatures. Arrhenius plots, calculated from C_2H_4 conversion rates, showed linear relationships for all the catalysts in the temperature range examined (Figure S2). The activation energy of the five Ni/ASA catalysts was calculated to be in the range of 20.9–29.3 kJ/mol and was not influenced by the Ni-loading or by the preparation method (Table S2). Furthermore, the activation energies of the catalysts were similar to previously reported values for Ni-exchanged ASA (16 kJ/mol) [23], $NiSO_4$/Al_2O_3 (16 kJ/mol) [40], Ni-SSZ-24 zeolite (33–37 kJ/mol) [49], Ni-Y zeolite (42–59 kJ/mol) [10], and Ni-Al-KIT-6 (15 kJ/mol) [38], suggesting that the structures of the active sites in these Ni catalysts were similar.
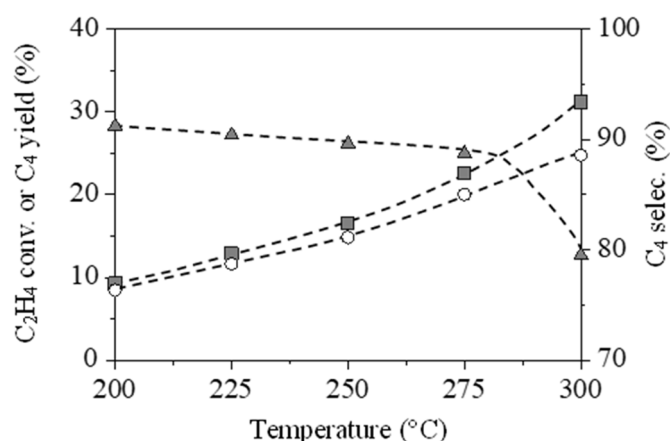
Figure 3. Effects of reaction temperature on C_2H_4 conversion (gray squares), C_4 yield (white circles), and C_4 selectivity (gray triangles) over a Ni/ASA catalyst prepared by an ion-exchange method of Ni-loading (Ni(1.1) IE). Conditions: Catalyst: 0.2 g, temperature: 200–300 °C, pressure: 0.1 MPa, C_2H_4: 20 mL/min, N_2: 20 mL/min.

To summarize, the catalytic activity of the Ni/ASA for EO was found to depend on the preparation method and Ni-loading, and the C_2H_4 conversion and C_4 yield decreased in the order of Ni IE > Ni Imp > Ni HP. The differences in catalytic activity were considered to originate from the different types of the Ni species; this is discussed in the next section.

2.2. Characterization of the Ni/ASA Catalysts and the Types of Active Ni Species

The Ni/ASA catalysts were characterized using several techniques. First, Ni contents of the Ni IE, Ni(2) Imp, and Ni(2) HP catalysts were analyzed using ICP-AES. Actual Ni-loading of Ni IE was 1.1 wt%, and those of Ni(2) Imp and Ni(2) HP were 1.9 and 2.1 wt%, respectively. In the Ni(2) Imp and Ni(2) HP catalysts, the Ni-loading obtained using ICP-AES was well consistent with that estimated based on the amount of $Ni(NO_3)_2 \cdot 6H_2O$ precursors used for the catalysts' preparation. Thus, it is believed that almost all of the Ni added was deposited on the ASA support when Ni/ASA catalysts were prepared using impregnation or one-step homogeneous precipitation.

The BET specific surface area, total pore volume, and average pore size of the Ni/ASA catalysts were compared with those of the ASA support (Table 2 and Figure S3). Ni-loading by ion-exchange had no effect on these three parameters (Table 2, Entry 2). However, in the Ni Imp catalysts (Table 2, Entries 3–10, and Figure S3a), the BET specific surface area decreased from 757 to 648 m^2/g with Ni-loading increasing from 0 to 4 wt%, and then became constant with further increases in Ni-loading; pore volume (0.56–0.65 cm^3/g) remained the same or slightly decreased; and average pore size (3.44–3.56 nm) remained the same or slightly increased. These results indicate that some of the entrances to the small pores in the ASA support were blocked during Ni-loading by impregnation. Similarly, in the Ni HP catalysts (Table 2, Entries 11–19, and Figure S3b), the BET specific surface area (663–794 m^2/g) slightly decreased, except for that of the Ni(1) HP catalyst; pore volume (0.59–0.69 cm^3/g) remained unchanged; and average pore size (3.41–3.90 nm) slightly increased, except for that of the Ni(1) HP catalyst. These results indicate that a small amount of aggregated Ni species was formed in the Ni HP catalysts and that this aggregate blocked some of the entrances to the small pores. The pore size distribution of all the Ni/ASA catalysts was similar to that of the ASA support (Figure S4). Together, these results show that both the amount of Ni and the preparation method had small effects on the pore structure of the Ni/ASA catalysts. In other words, the pore structure of the ASA support was mostly maintained, even at high Ni-loading. Therefore, we conclude that the variation of catalytic activity with Ni-loading and preparation method is attributable not to the pore structure of the catalysts but to the type of Ni species.

Table 2. Physicochemical properties of ASA support and Ni/ASA catalysts.

Entry	Catalysts	BET Specific Surface Area (m^2/g)	Pore Volume (cm^3/g)	Average Pore Size (nm)
1	ASA	757	0.65	3.45
2	Ni(1.1) IE	742	0.66	3.58
3	Ni(0.1) Imp	697	0.61	3.51
4	Ni(0.3) Imp	718	0.63	3.49
5	Ni(0.5) Imp	727	0.64	3.53
6	Ni(1) Imp	734	0.65	3.51
7	Ni(2) Imp	669	0.60	3.56
8	Ni(4) Imp	648	0.58	3.55
9	Ni(6) Imp	648	0.57	3.53
10	Ni(8) Imp	649	0.56	3.44
11	Ni(1) HP	794	0.68	3.41
12	Ni(2) HP	709	0.66	3.69
13	Ni(4) HP	703	0.63	3.61
14	Ni(6) HP	750	0.69	3.68
15	Ni(8) HP	677	0.61	3.60
16	Ni(10) HP	670	0.65	3.90
17	Ni(12) HP	665	0.59	3.54
18	Ni(16) HP	688	0.66	3.84
19	Ni(20) HP	663	0.59	3.59

XRD patterns of the ASA support and Ni/ASA catalysts are shown in Figure 4. From the XRD patterns of the low-Ni-loading catalysts (i.e., Ni(1) Imp, Ni(1.1) IE, Ni(1) HP and Ni(2) HP), the only peak characteristic of amorphous silica was observed at 15–40 degrees, indicating a high dispersion of Ni species on the ASA support. However, in the patterns of the high-Ni-loading samples, peaks attributable to Ni species were observed. The XRD patterns of the Ni Imp catalysts with high ($\geq$2 wt%) Ni-loading exhibited peaks at 37, 43, and 63 degrees, which corresponded to the (111), (200), and (220) planes of the NiO crystallites [11] (Figure 4a). This result clearly shows that, in the Ni Imp catalysts with high Ni-loading, some of the Ni species had aggregated to form large NiO particles. The NiO crystallite sizes of the Ni Imp catalysts were 9.2–11.6 nm and did not depend on Ni-loading (Table S3). In contrast, the XRD patterns of the Ni HP catalysts with high ($\geq$4 wt%) Ni-loading exhibited peaks at 34 and 61 degrees, which corresponded to the (110) and (300) planes of the NiSiO$_3$ crystallites [55] (Figure 4b). We attribute the formation of different Ni species between the Ni Imp and Ni HP catalysts to the different preparation methods. In the Ni Imp catalysts, the NiO particles were formed by calcining the Ni(NO$_3$)$_2$·6H$_2$O precursor adsorbed on the surface of the ASA support under an air atmosphere at 400 °C for 3 h. However, in the preparation of the Ni HP catalysts, the Ni^{2+} ions were deposited and the ASA support was formed simultaneously during aging at 90 °C for 2 days, resulting in the formation of a catalyst precursor characterized by a high dispersion of Ni species in the bulk and on the surface of the ASA support. Thus, it can be expected that highly dispersed Ni species react with the ASA to form NiSiO$_3$ during calcination at 500 °C for 6 h. The NiSiO$_3$ crystallite size of the Ni HP catalysts was 5.3–8.0 nm, which was smaller than the NiO crystallite size of the Ni Imp catalysts (Table S3).
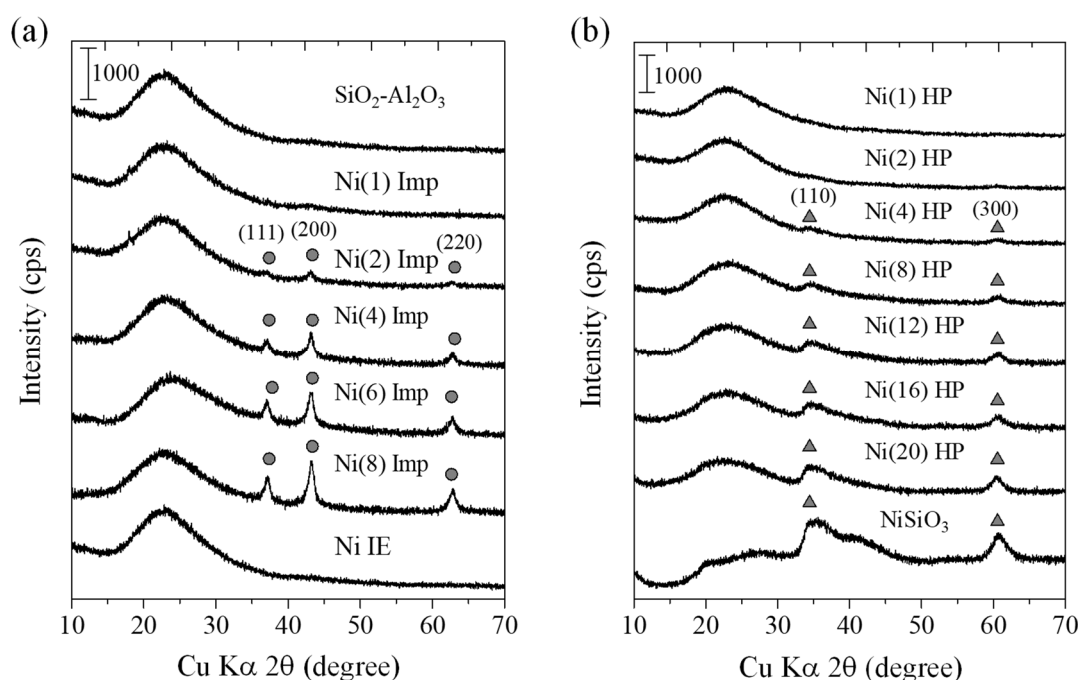
Figure 4. XRD patterns of Ni/ASA catalysts prepared by an (**a**) impregnation (Imp) or ion-exchange (IE), or (**b**) one-step homogeneous precipitation (HP) method of Ni-loading. Gray circles and triangles represent the diffraction lines of NiO and $NiSiO_3$, respectively.

FE-SEM observations of the ASA support and Ni/ASA catalysts were carried out to examine the differences in particle sizes and morphologies. At low magnification, various particles that had irregular shapes and sizes ranging from a few micrometers to 40 μm were observed in the ASA support and all the Ni/ASA catalysts (Figures 5, S5 and S6). Particle size and morphology were not influenced by the Ni-loading or preparation method. At high magnification, no clear differences were observed between the ASA support and the Ni/ASA catalysts, except for the Ni(8) Imp catalyst. The Ni(8) Imp catalyst (Figure 5f) was the only catalyst in which we observed the presence of NiO particles on the FE-SEM images; many of the NiO particles had a diameter smaller than 100 nm and were observed on the surface of the ASA support.

The H_2-TPR profiles of Ni/ASA, NiO, and $NiSiO_3$ are shown in Figure 6. The profiles of Ni/ASA catalysts are typically classified into three peaks: peaks at <400 °C are attributable to the reduction in large NiO particles displaying a low interaction with the support [13,26,31]; peaks at 400–600 °C are attributable to the reduction in small NiO nanoparticles interacting strongly with the support [26,31]; and peaks at >600 °C are attributable to the reduction in Ni cations in the ion-exchanged position [13,26,31] or in Ni silicate/aluminate [25,26]. In the present analysis, a small peak centered at 540 °C was observed in the profile of the Ni IE catalyst (Figure 6a). We attribute this peak to the reduction in isolated ion-exchanged Ni cations. The overall shape of the H_2-TPR profiles of the Ni Imp catalysts varied with Ni-loading. When Ni-loading was 1 wt%, the main reduction peak, corresponding to ion-exchanged Ni cations, was observed at 500–570 °C. Small shoulder peaks were also found at 400–500 °C, which were attributed to the reduction in small NiO particles interacting strongly with the ASA support. When Ni-loading was increased from 1 to 2 wt%, the area of these two peaks increased. Small peaks at 300–400 °C were also observed in the profile of the Ni(2) Imp; these were attributed to the reduction in bulk-like NiO particles. However, when Ni-loading was further increased to 8 wt%, the peak attributed to ion-exchanged Ni cations at 500–570 °C became small, whereas that attributed to small NiO particles at 400–500 °C became large. Peaks attributed to the reduction in bulk-like NiO particles at 300–400 °C also increased with increasing Ni-loading. Thus, we suggest that the main Ni species in the Ni Imp catalysts with low Ni-loading are

ion-exchanged Ni cations, and that of the Ni Imp catalysts with high Ni-loading are NiO particles.
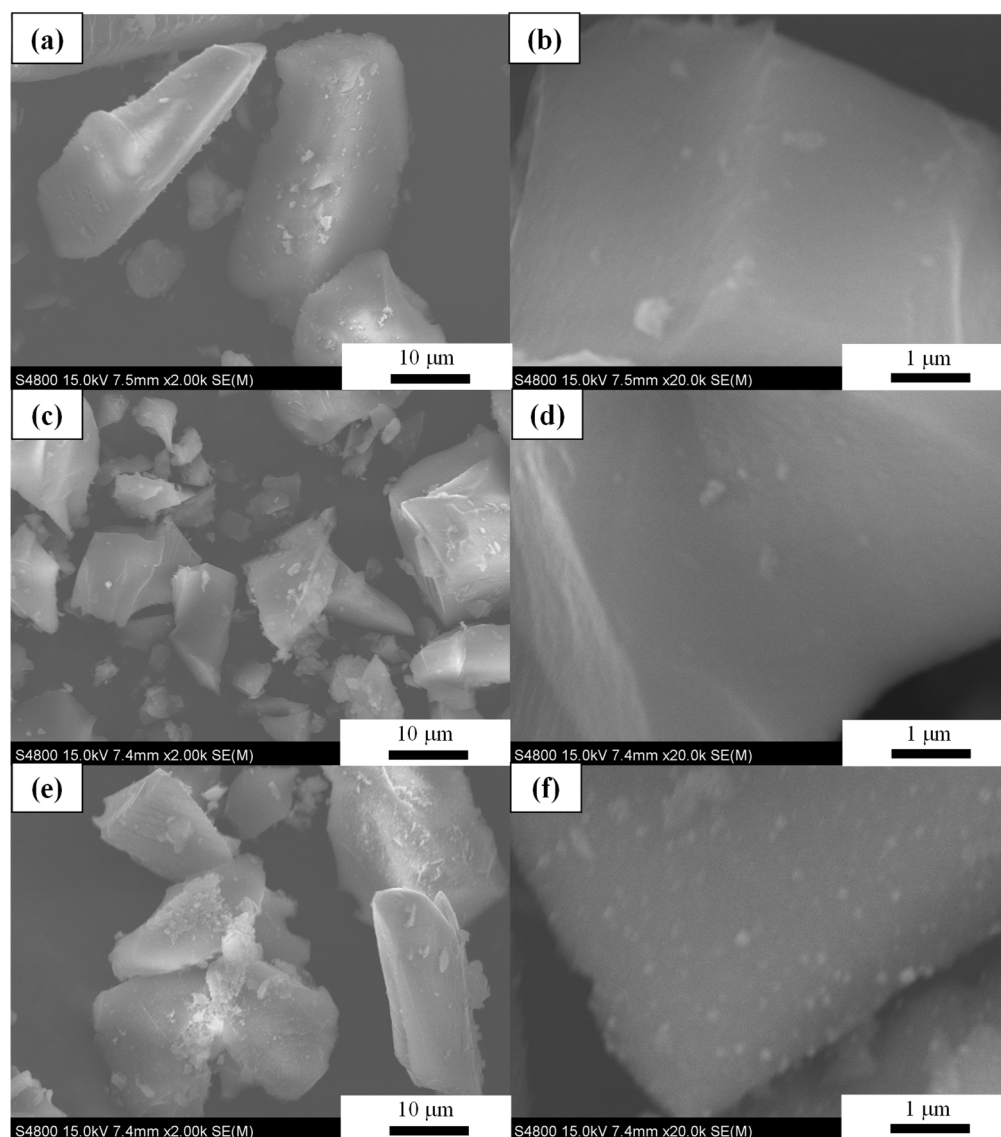

Figure 5. FE-SEM images of (**a**,**b**) ASA, (**c**,**d**) Ni(1) Imp, and (**e**,**f**) Ni(8) Imp.

A peak deconvolution of the H_2-TPR profiles of the Ni Imp catalysts was performed to estimate the amount of ion-exchanged Ni cations and of small and large NiO particles. The H_2-TPR profiles of all the Ni Imp catalysts were deconvoluted using three peaks, which were centered at 380 °C (α, peak attributed to bulk-like NiO particles), 490 °C (β, peak attributed to small NiO particles), and 530 °C (γ, peak attributed to ion-exchanged Ni cations) (Figure S7). The amounts of each Ni species were roughly calculated using the following formula: (amount of each Ni species) = (Ni-loading) × (area of each peak)/(total peak area). The amount of ion-exchanged Ni cations in the Ni Imp catalysts increased with increasing Ni-loading up to 2 wt%, after which it became constant in the Ni-loading range of 0.8–1.5 wt% (Table S4). This value was similar to the Ni-loading of the Ni IE catalyst, as measured using ICP-AES (1.1 wt%). In contrast, the amounts of small and large NiO particles tended to increase with an increase in Ni-loading. Together, these results show that the dispersion of Ni species in the Ni Imp catalysts decreased with increasing Ni-loading.
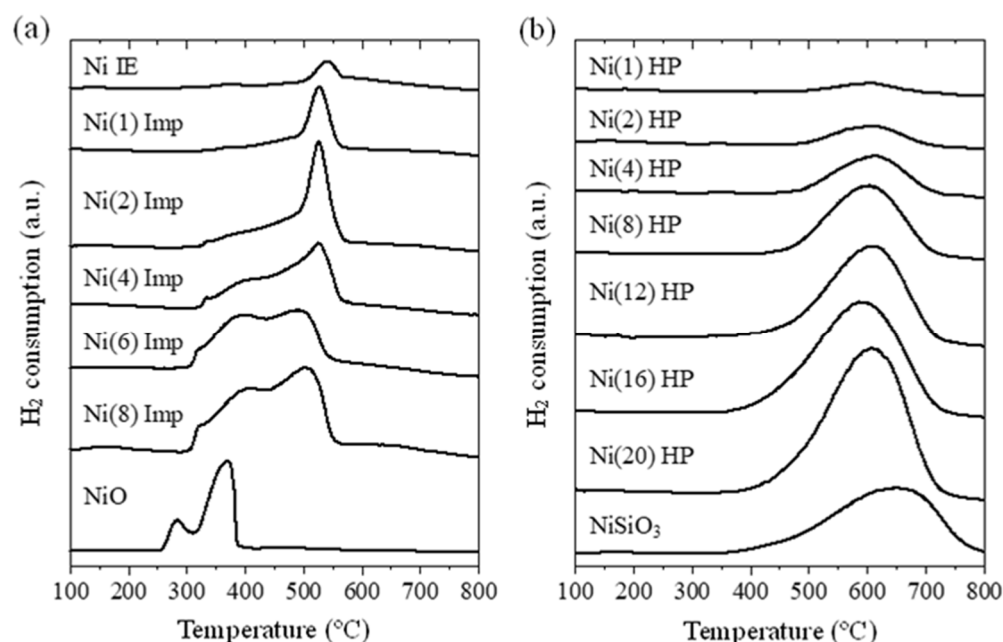
Figure 6. H_2-TPR profiles of Ni/ASA catalysts prepared by an (**a**) impregnation (Imp) or ion-exchange (IE), or (**b**) one-step homogeneous precipitation (HP) method of Ni-loading.

The overall shape of the H_2-TPR profiles of the Ni HP catalysts was different from that of the profiles of the Ni IE and Ni Imp catalysts, indicating that the Ni species in the Ni HP catalysts were different from those in the Ni IE and Ni Imp catalysts (Figure 6b). Namely, a symmetrical peak centered at around 600 °C was observed in the profiles of all the Ni HP catalysts regardless of Ni-loading. The H_2-TPR profile of the $NiSiO_3$ also showed a reduction peak in the same temperature range (450–750 °C), implying that the nature of the main Ni species in the Ni HP catalysts was similar to that of the Ni species in the $NiSiO_3$. However, the temperature of the peak maximum in the profiles of the Ni HP catalysts (600 °C) was lower than that in the profile of the $NiSiO_3$ (650 °C), indicating that the reducibility of the $NiSiO_3$ particles was enhanced by being supported on the ASA.

The NH_3-TPD profiles of the ASA support, the Ni/ASA catalysts, and the $NiSiO_3$ are shown in Figure 7. The profile of the ASA support showed a broad desorption peak at 100–800 °C, suggesting the existence of acidic sites with different strengths in the ASA support. From the profiles of the Ni IE and Ni Imp catalysts, not only broad desorption peaks originating from the ASA support but also desorption peaks originating from the Ni species were observed at 500–560 °C (Figure 7a). The profile of the Ni IE catalyst showed one desorption peak at 560 °C, which we attributed to ion-exchanged Ni cations. The profiles of the Ni(1) Imp and Ni(2) Imp catalysts showed two desorption peaks at 530 and 560 °C. The intensity of the peak at 530 °C increased with an increase in Ni-loading from 1 to 2 wt%, whereas the intensity of the peak at 560 °C did not change. We speculate that the peak at 530 °C originates from small NiO nanoparticles interacting strongly with the ASA support. The profiles of the Ni(4) Imp, Ni(6) Imp, and Ni(8) Imp catalysts showed a large desorption peak at 500 °C; the intensity of the peaks at 530 and 560 °C was much smaller than that of the peak at 500 °C in the profiles of these catalysts. We speculate that the peak at 500 °C originates from large NiO particles interacting weakly with the support. These results showed that the main Ni species in the Ni Imp catalysts changed from ion-exchanged Ni cations to large NiO particles with increasing Ni-loading. The amounts of weak (<400 °C), medium-strength (400–600 °C), and strong (>600 °C) acidic sites were estimated based on the amount of desorbed ammonia (Table S5). The amount of strong acidic sites in the Ni IE and Ni Imp catalysts was the same as that in the ASA support (Entries 1–7). However, the amount of weak acidic sites increased by 1.2–1.4 times and that of medium-strength acidic sites increased by 2.5–3.5 times after Ni-loading by ion-exchange

or impregnation. We attribute this large increase in the number of medium-strength acidic sites to the presence of ion-exchanged Ni cations and NiO particles.
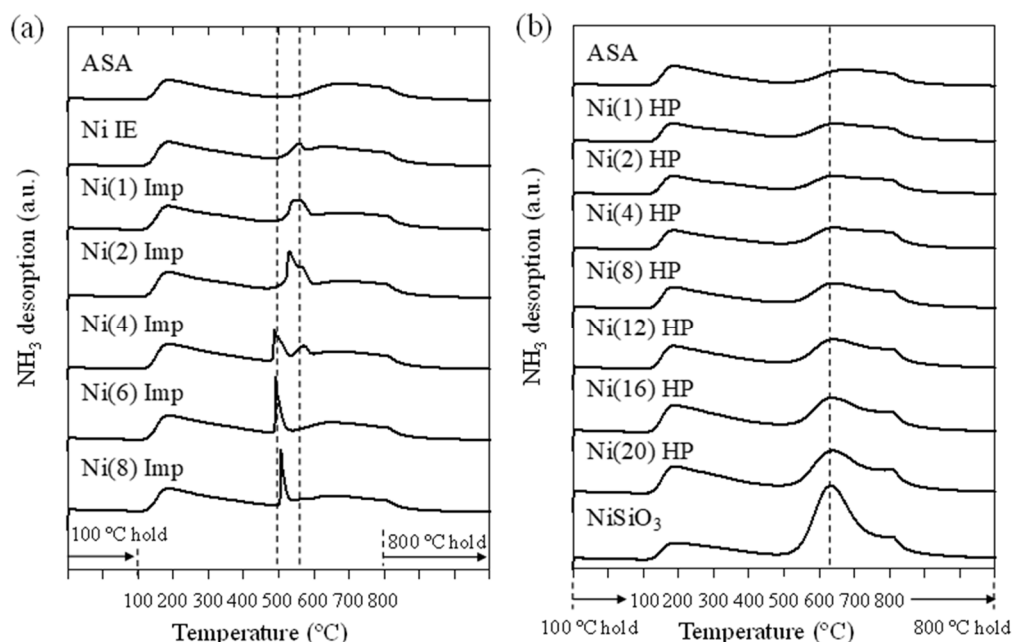

Figure 7. NH_3-TPD profiles of Ni/ASA catalysts prepared by an (**a**) impregnation (Imp) or ion-exchange (IE), or (**b**) one-step homogeneous precipitation (HP) method of Ni-loading.

In contrast, desorption peaks attributed to ion-exchanged Ni cations and NiO particles at 500–560 °C were not found in the NH_3-TPD profiles of the Ni HP catalysts (Figure 7b). Namely, the profiles of the Ni HP catalysts were very similar to that of the ASA support. However, the intensity of the peak at 635 °C increased with increasing Ni-loading and became closer to the peak intensity of the $NiSiO_3$. These results indicate that the Ni species in the Ni HP catalysts comprised only $NiSiO_3$ particles. The amounts of weak, medium-strength, and strong acidic sites in the Ni HP catalysts were also calculated based on the amount of desorbed ammonia (Table S5). The amounts of the three types of acidic sites monotonically increased with increasing Ni-loading (Entries 1 and 8–14). The increase in medium-strength and strong acidic sites was more pronounced than that of weak acidic sites.

Thus, we conclude the following from the results of the characterization of the Ni species in the Ni IE, Ni Imp, and Ni HP catalysts. In the Ni IE catalyst, the Ni species existed as ion-exchanged Ni cations. In the Ni Imp catalysts, the Ni species varied with Ni-loading: Ni Imp catalysts with low Ni-loading (<1 wt%) contained mainly ion-exchanged Ni cations; Ni Imp catalysts with moderate Ni-loading (1–2 wt%) contained both ion-exchanged Ni cations and small NiO particles; and Ni Imp catalysts with high Ni-loading (4–8 wt%) contained a mixture of ion-exchanged Ni cations, small NiO particles, and large, bulk-like NiO particles. In the Ni HP catalysts, the Ni species was always $NiSiO_3$, regardless of Ni-loading. The activity of the Ni Imp catalysts increased with increasing Ni-loading up to 0.5 wt% and then became constant with further increases (Figure 1a), which indicated that the ion-exchanged Ni cations were active for EO, whereas the small and large NiO particles were not active. The activity of the Ni HP catalysts showed an increasing-then-decreasing dependence on Ni-loading (Figure 1b), indicating that the $NiSiO_3$ was also active for EO but that its activity varied with the size of the $NiSiO_3$ particles.

C_2H_4-TPD measurements were carried out to examine the C_2H_4 adsorption properties of each Ni species. The profiles of the ASA support, Ni(8) Imp, Ni IE, and Ni(8) HP are shown in Figure 8. As described above, the Ni(8) Imp contained a large amount of NiO particles, the Ni IE contained only ion-exchanged Ni cations, and the Ni(8) HP contained

only NiSiO$_3$ particles. In Figure 8, the ASA support did not show any desorption peaks. However, the Ni(8) Imp showed three large desorption peaks centered at 180, 330, and 430 °C. The Ni IE and Ni(8) HP showed four large desorption peaks centered at 180, 330, 500–550, and 800 °C. Comparing three types of Ni/ASA catalysts, shape and intensity of peaks at 180 and 330 °C were very similar to each other, whereas those of peaks at >400 °C were much different. The Ni IE and Ni(8) HP showed desorption peaks at a higher temperature than the Ni(8) Imp, indicating that C$_2$H$_4$ adsorption to the ion-exchanged Ni cations and NiSiO$_3$ particles was stronger than that to the NiO particles. We believe that the differences in C$_2$H$_4$ adsorption properties originated from the different acid strengths of each Ni species. That is, the acidity of ion-exchanged Ni cations and NiSiO$_3$ particles was stronger than that of NiO particles (Figure 7), resulting in the stronger adsorption of C$_2$H$_4$ molecules to the former Ni species.
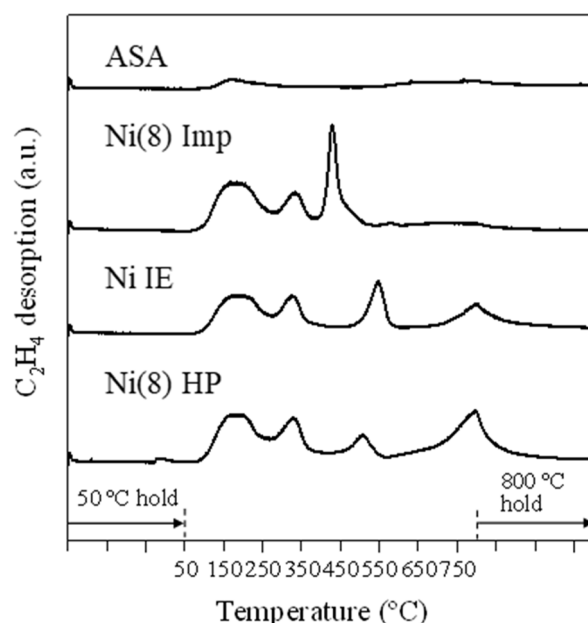

Figure 8. C$_2$H$_4$-TPD profiles of ASA support and Ni/ASA catalysts prepared by an impregnation (Imp), ion-exchange (IE), or one-step homogeneous precipitation (HP) method of Ni-loading.

The C$_2$H$_4$ conversion rate per gram of Ni was plotted against Ni-loading (Figure 9). The C$_2$H$_4$ conversion rate of the Ni Imp catalysts decreased with an increase in Ni-loading. This is because the amount of NiO particles, which were not active for EO, increased with increasing Ni-loading. The C$_2$H$_4$ conversion rate of the Ni HP catalysts also decreased with increasing Ni-loading, suggesting that the small NiSiO$_3$ particles were more active than the large NiSiO$_3$ particles. Comparing the C$_2$H$_4$ conversion rates of the Ni IE, Ni Imp, and Ni HP catalysts with similar Ni-loadings (1 wt%), we found that the C$_2$H$_4$ conversion rate of the Ni(1.1) IE and Ni(1) Imp was larger than that of the Ni(1) HP, indicating that ion-exchanged Ni cations were more active than NiSiO$_3$ particles.

The reasons for the high catalytic activity of ion-exchanged Ni cations were discussed as follows: the H$_2$-TPR profiles of the Ni/ASA catalysts showed that the interaction between the Ni species and the ASA support increased in the order of NiO particles < ion-exchanged Ni cations < NiSiO$_3$ particles (Figure 6). It is generally accepted that EO over Ni-aluminosilicate catalysts is greatly promoted by proximity of the Ni cations to the surface acidic sites of aluminosilicate support [31,42–44,53,54]. The roles of the acidic sites of the aluminosilicate support have not been clarified. However, Moussa et al. proposed that the acidic sites of the support enhanced the Lewis acidity of Ni species by electronic effect and thereby improved the ability of Ni sites to coordinate and activate C$_2$H$_4$ molecules [31]. Thus, we believe that, in the catalysts with a weak metal–support interaction (i.e., those

containing NiO particles), the distance between the Ni cations and surface acidic sites of the ASA support is large, and, thereby, these sites do not work cooperatively, resulting in a low catalytic activity for EO. In contrast, in catalysts with a strong metal–support interaction (i.e., those containing ion-exchanged Ni cations and $NiSiO_3$ nanoparticles), the Ni cations contact closely with the surface acidic sites of the ASA support, and, thereby, the ability of Ni sites to coordinate and activate C_2H_4 is largely improved. Moreover, the NH_3-TPD profiles showed that the acid strength of the Ni species increased in the order of NiO particles < ion-exchanged Ni cations < $NiSiO_3$ (Figure 7). The C_2H_4-TPD profiles also showed that C_2H_4 adsorption to the ion-exchanged Ni cations and $NiSiO_3$ particles was stronger than that to the NiO particles (Figure 8). Thus, we conclude that ion-exchanged Ni cations with a medium-strength (Lewis) acidity efficiently promote the adsorption and activation of ethylene and the desorption of products, resulting in a high catalytic activity. We are currently conducting several studies to clarify the structure and oxidation states of the ion-exchanged Ni cations in the Ni/ASA catalyst. For example, the diffuse reflectance UV-vis spectrum of the Ni IE catalyst under hydrated condition showed the adsorption bands at 13,600, 15,000, and 25,000 cm^{-1} (Figure S8). These bands corresponded to the d–d transitions of mononuclear octahedral $Ni^{2+}(H_2O)_6$ species and were also observed in the spectrum of a Ni-beta zeolite catalyst prepared using a liquid-state ion-exchange method [13,56]. Thus, we tentatively propose that active Ni species of the Ni IE catalyst may have a similar local structure to those of the Ni-beta zeolite catalyst. That is, the Ni^{2+} ions replace H^+ in bridged Si-OH-Al groups of the ASA support to form $[NiOH]^+$ species through the ion-exchange using a $Ni(NO_3)_2$ aqueous solution [14] (Figure S9). Then, the [NiOH]+ species are dehydrated through the calcination of the catalyst before reaction, resulting in the formation of bare Ni^{2+} ions that coordinate only to the lattice oxygen atoms of the support. We will continue to further study to understand the nature of the active Ni species of the Ni/ASA catalysts in more detail.
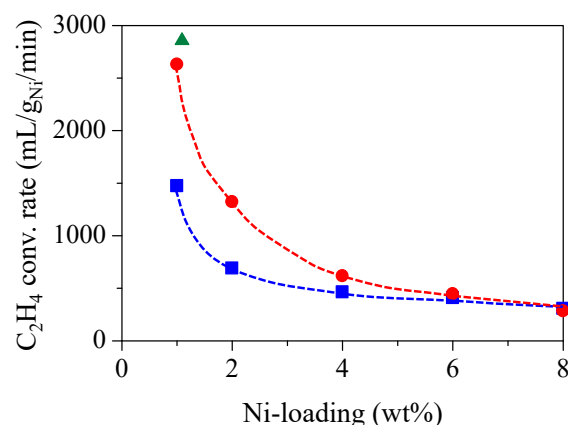

Figure 9. C_2H_4 conversion rate plotted against Ni-loading. Green triangles, red circles, and blue squares are the plots for catalysts prepared using an ion-exchange, impregnation, and one-step homogeneous precipitation method of Ni-loading, respectively. Conditions: Catalyst: 0.2 g, temperature: 300 °C, pressure: 0.1 MPa, C_2H_4: 20 mL/min, N_2: 20 mL/min.

3. Materials and Methods

3.1. Catalyst Synthesis

Chemical reagents and solvents for catalyst synthesis were obtained from Fujifilm Wako Pure Chemical Corporation (Osaka, Japan) and were used without any purification. The ASA support was synthesized using a homogeneous precipitation method similar to that described previously [54]. First, a metal precursor solution was prepared by dissolving tetraethyl orthosilicate (95.0+%, 19.62 g) and $Al(NO_3)_3\cdot9H_2O$ (98.0+%, 2.19 g) in EtOH (100 mL). Next, the precipitant solution was prepared by dissolving urea (99.0+%, 2.62 g) in deionized water (100 mL). Then, these two solutions were mixed and heated in an oil

bath at 90 °C for 2 days. After heating, the precipitant was recovered through filtration and washed with deionized water several times. Finally, the obtained solid was dried overnight at 110 °C and subsequently calcined under an air atmosphere at 500 °C for 6 h. The Al_2O_3 content was fixed at 3 mol%.

The Ni/ASA catalysts were prepared using the following three methods:

Impregnation: The ASA support was suspended in a $Ni(NO_3)_2$ aqueous solution, and the obtained slurry was dried on a hot plate. The Ni-loading was varied from 0.1 to 8 wt%. After impregnation, the samples were dried overnight at 110 °C in an oven and subsequently calcined under an air atmosphere at 400 °C for 3 h.

One-step homogeneous precipitation: Tetraethyl orthosilicate, $Al(NO_3)_3 \cdot 9H_2O$, and $Ni(NO_3)_2 \cdot 6H_2O$ were dissolved in EtOH (100 mL); the sum of the concentrations of Si^{4+}, Al^{3+}, and Ni^{2+} ions was maintained at 1 mol/L. Next, urea was dissolved in deionized water (100 mL); the amount of urea was five times what was needed for precipitating Al^{3+} and Ni^{2+} ions. Then, these two solutions were mixed and heated in an oil bath at 90 °C for 2 days. The precipitant was recovered through filtration and washed with deionized water several times. Finally, the obtained solid was dried overnight at 110 °C and subsequently calcined under an air atmosphere at 500 °C for 6 h. The Ni-loading was varied from 1 to 20 wt%.

Ion-exchange: The ASA powder was dispersed in a 1 mol/L $Ni(NO_3)_2$ aqueous solution (1.0 g solid per 10 mL solution) and stirred at 70 °C for 4 h. The solid was recovered through filtration, followed by washing with deionized water several times to eliminate the non-exchanged Ni species, and drying overnight at 110 °C. These operations were carried out three times. After the final exchange cycle, the Ni-exchanged catalyst was calcined under an air atmosphere at 400 °C for 3 h.

The catalysts prepared with impregnation, one-step homogeneous precipitation, and ion-exchange are hereafter referred to as Ni(*x*) Imp, Ni(*x*) HP, and Ni(*x*) IE, respectively, where *x* indicates the Ni-loading.

The $NiSiO_3$ was prepared following the same procedure as the one-step homogeneous precipitation method described above, except that $Al(NO_3)_3 \cdot 9H_2O$ was not added.

3.2. Characterization Techniques

The nitrogen adsorption and desorption isotherms were acquired at −196 °C using an ASAP 2020 automatic analyzer (Micromeritics, Norcross, GA, USA). Before analysis, the sample (0.10–0.20 g) was outgassed at 350 °C and vacuumed for 4 h. The specific surface area was calculated from the Brunauer–Emmett–Teller (BET) analysis of absorption data in the relative N_2 pressure range of 0.05–0.30. The pore volume was evaluated using the adsorption volume of N_2 gas at a relative N_2 pressure of 0.99. The pore size distribution was estimated from the Barrett–Joyner–Halenda (BJH) analysis of the desorption data.

The X-ray powder diffraction (XRD) pattern was obtained on a D8 ADVANCE diffractometer (Bruker AXS, Billerica, MA, USA) using Ni-filtered Cu Kα radiation (λ = 1.5418 Å). The diffractograms were recorded in the 2θ range of 10–70 degree with steps of 0.02 degree at 40 kV and 40 mA. The crystallite sizes of NiO and $NiSiO_3$ were estimated from the diffraction lines at 43.2 and 60.7 degrees, respectively, using the Scherrer equation.

The field-emission scanning electron microscope (FE-SEM) image was obtained on a S-4800 microscope (Hitachi, Tokyo, Japan) operated at 15 kV.

The H_2 temperature-programmed reduction (H_2-TPR) was performed using a BELCAT-B auto-chemisorption system (MicrotracBEL Corp., Osaka, Japan), equipped with a thermal conductivity detector (TCD). The sample (0.10 g) was loaded into a U-shaped quartz cell and the temperature was increased up to 800 °C (heating rate, 5 °C/min) under 10% H_2/Ar flow (30 mL/min). A downstream trap containing the molecular sieve 5A was used to remove the water formed during analysis. The peak deconvolution was carried out with the ChemMaster analysis software (Version 1.4.4, MicrotracBEL Corp., Osaka, Japan) using Gaussian functions.

The NH_3 temperature-programmed desorption (NH_3-TPD) was carried out using a BELCAT-B auto-chemisorption system (MicrotracBEL Corp., Osaka, Japan). The sample (0.10–0.15 g) was preheated at 500 °C for 60 min under He gas flow (30 mL/min), followed by cooling to 100 °C under flowing He. Next, the adsorption of ammonia was carried out at 100 °C in flowing 5% NH_3/He (30 mL/min) for 30 min. Then, the sample was purged with He (30 mL/min) at the same temperature for 60 min to remove the physisorbed ammonia. Finally, a NH_3-TPD experiment was conducted by increasing the temperature to 800 °C (heating rate, 10 °C/min) under flowing He (30 m/min). The amounts of weak (<400 °C), medium-strength (400–600 °C), and strong (>600 °C) acidic sites were estimated from the amount of desorbed ammonia.

The C_2H_4 temperature-programmed desorption (C_2H_4-TPD) was carried out using a BELCAT II auto-chemisorption system (MicrotracBEL Corp., Osaka, Japan), equipped with a mass spectrometer. The sample (0.10 g) was preheated at 500 °C for 60 min under He gas flow (30 mL/min), followed by cooling to 50 °C under flowing He. Next, the adsorption of C_2H_4 was carried out at 50 °C in flowing C_2H_4 gas (30 mL/min) for 30 min. Then, the sample was purged with He (30 mL/min) at the same temperature for 60 min to remove the physisorbed C_2H_4. Finally, a C_2H_4-TPD experiment was conducted by increasing the temperature to 800 °C (heating rate, 10 °C/min) under flowing He (30 mL/min).

The Ni content of the Ni(2) Imp, Ni(2) HP, and Ni IE catalysts was analyzed using inductively-coupled plasma–atomic emission spectroscopy (ICP-AES, ICPE-9800, Shimadzu, Kyoto, Japan). The solution used for ICP-analysis was prepared by dissolving the catalyst powder in hydrofluoric acid.

The diffuse reflectance UV-vis spectra were recorded on a UV-2600 spectrometer (Shimazu, Kyoto, Japan) equipped with an integrating sphere in the spectral range of 12,500–50,000 cm^{-1} (200–800 nm). $BaSO_4$ was used as a reference sample to measure the baseline spectrum.

3.3. Activity Test for Ethylene Oligomerization

Reaction experiments were carried out using a continuous-flow fixed-bed reactor in similar ways to previous studies [53,54]. The catalyst powder (0.20 g), which was granulated to the particle size of 0.36–0.71 mm, was mounted on the quartz reactor and preheated in situ at 450 °C for 60 min under N_2 flow (20 mL/min). Then, the reactor was cooled down to the desired temperature under N_2 flow and switched to the reaction gas. Typically, the reaction was carried out at 300 °C and 0.1 MPa. The reaction gas was a mixture of C_2H_4 and N_2. The flow rates of C_2H_4 and N_2 were 20 mL/min and 20 mL/min, respectively. The reaction time was 40 min. The oligomerization products were measured using an online gas chromatograph (GC-2014, Shimadzu, Kyoto, Japan) that was equipped with a flame ionization detector (FID) and a capillary column (Rtx-1, Restek, Bellefonte, PA, USA). Reaction experiments were carried out three times for each catalyst to confirm the reproducibility, and average values were employed as the experimental data.

4. Conclusions

In this study, we prepared NiO/SiO_2-Al_2O_3 (Ni/ASA) catalysts using three methods of Ni-loading—ion-exchange (IE), impregnation (Imp), and homogeneous precipitation (HP)—and then we evaluated their catalytic performance for ethylene oligomerization (EO). The Ni/ASA catalyst prepared using IE showed the highest activity (i.e., highest C_2H_4 conversion and C_4 yield); the catalysts prepared using Imp showed the second highest activity; and the catalysts prepared using HP showed the lowest activity. Characterization by XRD, FE-SEM, H_2-TPR, NH_3-TPD, and C_2H_4-TPD showed that the main Ni species in the Ni/ASA catalysts prepared using IE, Imp, and HP were as follows: ion-exchange Ni cations; a mixture of ion-exchange Ni cations and NiO particles; and $NiSiO_3$ particles, respectively. In the Ni Imp catalysts, the ratio of ion-exchange Ni cations decreased but that of NiO particles increased with increasing Ni-loading. The comparison of the C_2H_4 conversion rates of each Ni species indicated the following: ion-exchanged Ni species

were highly active; NiO particles were not active; and NiSiO$_3$ particles showed moderate activity for EO. The high dispersion and medium-strength (Lewis) acidity of ion-exchanged Ni cations contributed to promoting the adsorption and activation of ethylene and the desorption of products, resulting in a superior catalytic performance for EO.

Supplementary Materials: The following supporting information can be downloaded at: https://www.mdpi.com/article/10.3390/catal13091303/s1, Figure S1: Time course of C$_2$H$_4$ conversion over representative Ni/ASA catalysts prepared by an ion-exchange, impregnation, or one-step homogeneous precipitation method of Ni-loading; Figure S2: Arrhenius plots for conversion of C$_2$H$_4$ over Ni/ASA catalyst prepared by an ion-exchange method of Ni-loading; Figure S3: BET specific surface area, average pore size, and pore volume of Ni/ASA catalysts prepared by an (a) impregnation or (b) one-step homogeneous precipitation method of Ni-loading; Figure S4: Pore size distribution of Ni/ASA catalysts prepared by an (a) impregnation or ion-exchange, or (b) one-step homogeneous precipitation method of Ni-loading; Figure S5: FE-SEM images of Ni/ASA catalyst prepared by an ion-exchange method of Ni-loading; Figure S6: FE-SEM images of representative Ni/ASA catalysts prepared by a one-step homogeneous precipitation method of Ni-loading: (a,b) Ni(1) HP, (c,d) Ni(8) HP, (e,f) Ni(16) HP; Figure S7: Peak deconvolution of the H$_2$-TPR profile of a representative Ni/ASA catalyst prepared by an impregnation method of Ni-loading; Figure S8: Diffuse reflectance UV-vis spectra of the ASA support and Ni/ASA catalysts prepared by an ion-exchange, impregnation, or one-step homogeneous precipitation method of Ni-loading; Figure S9: Proposed structure of ion-exchanged Ni cation in Ni/ASA catalyst; Table S1: Comparison of catalytic activity of Ni-containing heterogeneous catalysts in EO [1,57,58]; Table S2: Activation energies of representative Ni/ASA catalysts; Table S3: Crystallite size of NiO and NiSiO$_3$, as measured by XRD; Table S4: Deconvolution of H$_2$-TPR profiles of Ni/ASA catalysts prepared by an impregnation method; Table S5: Amounts of acidic sites in ASA and Ni/ASA, as calculated from NH$_3$-TPD profiles.

Author Contributions: Conceptualization, S.Y. and H.O.; methodology, K.S. and T.F.; investigation, K.S.; data curation, K.S.; writing—original draft preparation, K.S.; writing—review and editing, S.Y., H.O. and T.F.; visualization, K.S.; supervision, T.F.; project administration, S.Y. and H.O. All authors have read and agreed to the published version of the manuscript.

Data Availability Statement: Not applicable.

Conflicts of Interest: The authors declare no conflict of interest.

References

1. Finiels, A.; Fajula, F.; Hulea, V. Nickel-Based Solid Catalysts for Ethylene Oligomerization—A Review. *Catal. Sci. Technol.* **2014**, *4*, 2412–2426. [CrossRef]
2. Joshi, R.; Saxena, A.; Gounder, R. Mechanistic Insights into Alkene Chain Growth Reactions Catalyzed by Nickel Active Sites on Ordered Microporous and Mesoporous Supports. *Catal. Sci. Technol.* **2020**, *10*, 7101–7123. [CrossRef]
3. Olivier-Bourbigou, H.; Breuil, P.A.R.; Magna, L.; Michel, T.; Pastor, M.F.E.; Delcroix, D. Nickel Catalyzed Olefin Oligomerization and Dimerization. *Chem. Rev.* **2020**, *120*, 7919–7983. [CrossRef]
4. Betz, M.; Fuchs, C.; Zevaco, T.A.; Arnold, U.; Sauer, J. Production of Hydrocarbon Fuels by Heterogeneously Catalyzed Oligomerization of Ethylene: Tuning of the Product Distribution. *Biomass Bioenergy* **2022**, *166*, 106595. [CrossRef]
5. Seufitelli, G.V.S.; Gustafson, R. Novel Ni-SIRAL Catalyst for Heterogeneous Ethylene Oligomerization. *Ind. Eng. Chem. Res.* **2022**, *61*, 4286–4299. [CrossRef]
6. Mohamed, H.O.; Abed, O.; Zambrano, N.; Castaño, P.; Hita, I. A Zeolite-Based Cascade System to Produce Jet Fuel from Ethylene Oligomerization. *Ind. Eng. Chem. Res.* **2022**, *61*, 15880–15892. [CrossRef]
7. McGuinness, D.S. Olefin Oligomerization via Metallacycles: Dimerization, Trimerization, Tetramerization, and Beyond. *Chem. Rev.* **2011**, *111*, 2321–2341. [CrossRef]
8. Breuil, P.R.; Magna, L.; Olivier-Bourbigou, H. Role of Homogeneous Catalysis in Oligomerization of Olefins: Focus on Selected Examples Based on Group 4 to Group 10 Transition Metal Complexes. *Catal. Lett.* **2015**, *145*, 173–192. [CrossRef]
9. Heveling, J.; Beek, A.V.D.; Pender, M.D. Oligomerization of Ethene over Nickel-Exchanged Zeolite Y into a Diesel-Range Product. *Appl. Catal.* **1988**, *42*, 325–336. [CrossRef]
10. Ng, F.T.T.; Creaser, D.C. Ethylene Dimerization: Kinetics and Selectivity for 1-Butene. *Stud. Surf. Sci. Catal.* **1992**, *73*, 123–131.

11. Martínez, A.; Arribas, M.A.; Concepción, P.; Moussa, S. New Bifunctional Ni–H-Beta Catalysts for the Heterogeneous Oligomerization of Ethylene. *Appl. Catal. A: Gen.* **2013**, *467*, 509–518. [CrossRef]

12. Moussa, S.; Concepción, P.; Arribas, M.A.; Martínez, A. Nature of Active Nickel Sites and Initiation Mechanism for Ethylene Oligomerization on Heterogeneous Ni-Beta Catalysts. *ACS Catal.* **2018**, *8*, 3903–3912. [CrossRef]

13. Lee, K.; Hong, S.B. Ethene Dimerization over Ni-Beta Catalysts Prepared by Solid-State Ion exchange. *Appl. Catal. A: Gen.* **2021**, *615*, 118059. [CrossRef]

14. McCaig, J.; Lamb, H.H. Ni-H-Beta Catalysts for Ethylene Oligomerization: Impact of Parent Cation on Ni Loading, Speciation, and Siting. *Catalysts* **2022**, *12*, 824. [CrossRef]

15. Yamamura, M.; Chaki, K.; Wakatsuki, T.; Okado, H.; Fujimoto, K. Synthesis of ZSM-5 Zeolite with Small Crystal Size and Its Catalytic Performance for Ethylene Oligomerization. *Zeolites* **1994**, *14*, 643–649. [CrossRef]

16. Ganjkhanlou, Y.; Berlier, G.; Groppo, E.; Borfecchia, E.; Bordiga, S. In Situ Investigation of the Deactivation Mechanism in Ni-ZSM5 During Ethylene Oligomerization. *Top Catal.* **2017**, *60*, 1664–1672. [CrossRef]

17. Lallemand, M.; Rusu, O.A.; Dumitriu, E.; Finiels, A.; Fajula, F.; Hulea, V. Ni-MCM-36 and Ni-MCM-22 Catalysts for the Ethylene Oligomerization. *Stud. Surf. Sci. Catal.* **2008**, *174*, 1139–1142.

18. Lallemand, M.; Rusu, O.A.; Dumitriu, E.; Finiels, A.; Fajula, F.; Hulea, V. NiMCM-36 and NiMCM-22 Catalysts for the Ethylene Oligomerization: Effect of Zeolite Texture and Nickel Cations/Acid Sites Ratio. *Appl. Catal. A Gen.* **2008**, *338*, 37–43. [CrossRef]

19. Espinoza, R.L.; Snel, R.; Korf, C.J.; Nicolaides, C.P. Catalytic Oligomerization of Ethene over Nickel-Exchanged Amorphous Silica-Aluminas; Effect of the Acid Strength of the Support. *Appl. Catal.* **1987**, *29*, 295–303. [CrossRef]

20. Espinoza, R.L.; Nicolaides, C.P.; Korf, C.J.; Snel, R. Catalytic Oligomerization of Ethene over Nickel-Exchanged Amorphous Silica-Alumina; Effect of the Nickel Concentration. *Appl. Catal.* **1987**, *31*, 259–266. [CrossRef]

21. Espinoza, R.L.; Korf, C.J.; Nicolaides, C.P.; Snel, R. Catalytic Oligomerization of Ethene over Nickel-Exchanged Amorphous Silica-Alumina; Effect of the Reaction Conditions and Modelling of the Reaction. *Appl. Catal.* **1987**, *29*, 175–184. [CrossRef]

22. Heveling, J.; Nicolaides, C.P.; Scurrell, M.S. Catalysts and Conditions for the Highly Efficient, Selective and Stable Heterogeneous Oligomerisation of Ethylene. *Appl. Catal. A Gen.* **1998**, *173*, 1–9. [CrossRef]

23. Heydenrych, M.D.; Nicolaides, C.P.; Scurrell, M.S. Oligomerization of Ethene in a Slurry Reactor Using a Nickel(II)-Exchanged Silica–Alumina Catalyst. *J. Catal.* **2001**, *197*, 49–57. [CrossRef]

24. Toch, K.; Thybaut, J.W.; Marin, G.B. Ethene Oligomerization on Ni-SiO$_2$-Al$_2$O$_3$: Experimental Investigation and Single-Event MicroKinetic Modeling. *Appl. Catal. A Gen.* **2015**, *489*, 292–304. [CrossRef]

25. Yoon, J.S.; Park, M.B.; Kim, Y.; Hwang, D.W.; Chae, H. Effect of Metal Oxide–Support Interactions on Ethylene Oligomerization over Nickel Oxide/Silica–Alumina Catalysts. *Catalysts* **2019**, *9*, 933. [CrossRef]

26. Khudhair, A.A.; Bouchmella, K.; Andrei, R.D.; Mehdi, A.; Mutin, P.H.; Hulea, V. One-Step Non-Hydrolytic Sol-Gel Synthesis of Mesoporous SiO$_2$-Al$_2$O$_3$-NiO Catalysts for Ethylene Oligomerization. *Microporous Mesoporous Mater.* **2021**, *322*, 111165. [CrossRef]

27. Xu, J.; Wang, R.; Zhang, Y.; Li, L.; Yan, W.; Wang, J.; Liu, G.; Su, X.; Huang, Y.; Zhang, T. Identification of the Structure of Ni Active Sites for Ethylene Oligomerization on an Amorphous Silica-Alumina Supported Nickel Catalyst. *Chin. J. Catal.* **2021**, *42*, 2181–2188. [CrossRef]

28. Aid, A.; Andrei, R.D.; Amokrane, S.; Cammarano, C.; Nibou, D.; Hulea, V. Ni-Exchanged Cationic Clays as Novel Heterogeneous Catalysts for Selective Ethylene Oligomerization. *Appl. Clay Sci.* **2017**, *146*, 432–438. [CrossRef]

29. Hulea, V.; Fajula, F. Ni-Exchanged AlMCM-41—An Efficient Bifunctional Catalyst for Ethylene Oligomerization. *J. Catal.* **2004**, *225*, 213–222. [CrossRef]

30. Agirrezabal-Telleria, I.; Iglesia, E. Stabilization of Active, Selective, and Regenerable Ni-Based Dimerization Catalysts by Condensation of Ethene within Ordered Mesopores. *J. Catal.* **2017**, *352*, 505–514. [CrossRef]

31. Moussa, S.; Concepción, P.; Arribas, M.A.; Martínez, A. The Nature of Active Ni Sites and the Role of Al Species in the Oligomerization of Ethylene on Mesoporous Ni-Al-MCM-41 Catalysts. *Appl. Catal. A Gen.* **2020**, *608*, 117831. [CrossRef]

32. Li, W.; Zhou, C.; Li, W.; Ge, L.; Yu, G.; Qiu, M.; Chen, X. Tuning the Ni Site Location of Bifunctional Ni-Based Catalysts for Improving the Performance in Ethylene Oligomerization. *New J. Chem.* **2022**, *46*, 9461–9469. [CrossRef]

33. Andrei, R.D.; Mureseanu, M.; Popa, M.I.; Cammarano, C.; Fajula, F.; Hulea, V. Ni-Exchanged AlSBA-15 Mesoporous Materials as Outstanding Catalysts for Ethylene Oligomerization. *Eur. Phys. J. Special Topics* **2015**, *224*, 1831–1841. [CrossRef]

34. Andrei, R.D.; Popa, M.I.; Fajula, F.; Hulea, V. Heterogeneous Oligomerization of Ethylene over Highly Active and Stable Ni-AlSBA-15 Mesoporous Catalysts. *J. Catal.* **2015**, *323*, 76–84. [CrossRef]

35. Andrei, R.D.; Popa, M.I.; Cammaranoa, C.; Hulea, V. Nickel and Molybdenum Containing Mesoporous Catalysts for Ethylene Oligomerization and Metathesis. *New J. Chem.* **2016**, *40*, 4146–4152. [CrossRef]

36. Jan, O.; Song, K.; Dichiara, A.; Resende, F.L.P. Oligomerization of Supercritical Ethylene over Nickel-Based Silica-Alumina Catalysts. *Chem. Eng. Sci.* **2019**, *197*, 212–222. [CrossRef]

37. Beucher, R.; Cammarano, C.; Rodríguez-Castellón, E.; Hulea, V. Direct Conversion of Ethylene to Propylene over Ni- and W-Based Catalysts: An Unprecedented Behaviour. *Catal. Commun.* **2020**, *144*, 106091. [CrossRef]

38. Beucher, R.; Hulea, V.; Cammarano, C. Kinetic and Mechanistic Insights into Ni-AlKIT-6 Catalyzed Ethylene Oligomerization. *React. Chem. Eng.* **2022**, *7*, 133–141. [CrossRef]

39. Cai, T.; Cao, D.; Song, Z.; Li, L. Catalytic Behavior of NiSO$_4$/γ-Al$_2$O$_3$ for Ethene Dimerization. *Appl. Catal. A Gen.* **1993**, *95*, Ll–L7. [CrossRef]

40. Zhang, Q.; Dalla Lana, I.G. An Analysis of Mass Transfer and Kinetics during Ethylene Oligomerization over Nickel/Sulfated Alumina Catalyst in a Slurry Reactor. *Chem. Eng. Sci.* **1997**, *52*, 4187–4195. [CrossRef]

41. Cai, T. Studies of a New Alkene Oligomerization Catalyst Derived from Nickel Sulfate. *Catal. Today* **1999**, *51*, 153–160. [CrossRef]

42. Sohn, J.R.; Park, W.C.; Kim, H.W. Characterization of Nickel Sulfate Supported on γ-Al$_2$O$_3$ for Ethylene Dimerization and Its Relationship to Acidic Properties. *J. Catal.* **2002**, *209*, 69–74. [CrossRef]

43. Sohn, J.R.; Park, W.C.; Shin, D.C. Characterization of Nickel Sulfate Supported on SiO$_2$ for Ethylene Dimerization and Promoting Effect of Al$_2$O$_3$ on Catalytic Activity. *J. Mol. Catal. A Chem.* **2006**, *256*, 156–163. [CrossRef]

44. Sohn, J.R.; Lee, S.H. Effect of TiO$_2$–ZrO$_2$ Composition on Catalytic Activity of Supported NiSO$_4$ for Ethylene Dimerization. *Appl. Catal. A Gen.* **2007**, *321*, 27–34. [CrossRef]

45. Shin, M.; Suh, Y. Ethylene Oligomerization over SiO$_2$–Al$_2$O$_3$ Supported Ni$_2$P Catalyst. *ChemCatChem* **2020**, *12*, 135–140. [CrossRef]

46. Shin, M.; Jeong, H.; Park, M.; Suh, Y. Benefits of the SiO$_2$-Supported Nickel Phosphide Catalyst on Ethylene Oligomerization. *Appl. Catal. A Gen.* **2020**, *591*, 117376. [CrossRef]

47. Henry, R.; Komurcu, M.; Ganjkhanlou, Y.; Brogaard, R.Y.; Lu, L.; Jens, K.; Berlier, G.; Olsbye, U. Ethene Oligomerization on Nickel Microporous and Mesoporous-Supported Catalysts: Investigation of the Active Sites. *Catal. Today* **2018**, *299*, 154–163. [CrossRef]

48. Moussa, S.; Arribas, M.A.; Concepción, P.; Martínez, A. Heterogeneous Oligomerization of Ethylene to Liquids on Bifunctional Ni-Based Catalysts: The Influence of Support Properties on Nickel Speciation and Catalytic Performance. *Catal. Today* **2016**, *277*, 78–88. [CrossRef]

49. Brogaard, R.Y.; Kømurcu, M.; Dyballa, M.M.; Botan, A.; Speybroeck, V.V.; Olsbye, U.; Wispelaere, K.D. Ethene Dimerization on Zeolite-Hosted Ni Ions: Reversible Mobilization of the Active Site. *ACS Catal.* **2019**, *9*, 5645–5650. [CrossRef]

50. Choo, H.; Kevan, L. Catalytic Study of Ethylene Dimerization on Ni(II)-Exchanged Clinoptilolite. *J. Phys. Chem. B* **2001**, *105*, 6353–6360. [CrossRef]

51. Mlinar, A.N.; Shylesh, S.; Ho, O.C.; Bell, A.T. Propene Oligomerization using Alkali Metal- and Nickel-Exchanged Mesoporous Aluminosilicate Catalysts. *ACS Catal.* **2014**, *4*, 337–343. [CrossRef]

52. Mlinar, A.N.; Baur, G.B.; Bong, G.G.; Getsoian, A.; Bell, A.T. Propene Oligomerization over Ni-exchanged Na-X Zeolites. *J. Catal.* **2012**, *296*, 156–164. [CrossRef]

53. Shimura, K.; Yoshida, S.; Oikawa, H.; Fujitani, T. Ethylene Oligomerization over NiO$_x$/SiO$_2$-Al$_2$O$_3$ Catalysts Prepared by a Coprecipitation Method. *Mol. Catal.* **2022**, *528*, 112478. [CrossRef]

54. Shimura, K.; Yoshida, S.; Oikawa, H.; Fujitani, T. Preparation of NiO$_x$/SiO$_2$-Al$_2$O$_3$ Catalysts by a Homogenous Precipitation Method and Their Catalytic Activity for Ethylene Oligomerization. *Microporous Mesoporous Mater.* **2022**, *338*, 111955. [CrossRef]

55. Yuan, S.; Zhao, L. Hierarchical Core–Shell Structured Fe$_3$O$_4$@NiSiO$_3$ Magnetic Microspheres: Preparation, Characterization, and Adsorption of Methylene Blue from Aqueous Solution. *RSC Adv.* **2016**, *6*, 49769–49776. [CrossRef]

56. Joshi, R.; Zhang, G.; Miller, J.T.; Gounder, R. Evidence for the Coordination−Insertion Mechanism of Ethene Dimerization at Nickel Cations Exchanged onto Beta Molecular Sieves. *ACS Catal.* **2018**, *8*, 11407–11422. [CrossRef]

57. Hulea, V. Toward Platform Chemicals from Bio-Based Ethylene: Heterogeneous Catalysts and Processes. *ACS Catal.* **2018**, *8*, 3263–3279. [CrossRef]

58. Heveling, J.; Nicolaides, C.P. Chain-Length Distributions Obtained over Nickel(II)-Exchanged or Impregnated Silica–Alumina Catalysts for the Oligomerization of Lower Alkenes. *Catal. Lett.* **2006**, *107*, 117–121. [CrossRef]